Role of Filler Shape and Connectivity on the Viscoelastic Behavior in Polymer Nanocomposites

ARTICLE *in* MACROMOLECULES · AUGUST 2015

Impact Factor: 5.8 · DOI: 10.1021/acs.macromol.5b00962

6 AUTHORS, INCLUDING:

Dan Zhao

Columbia University

6 PUBLICATIONS **11** CITATIONS

SEE PROFILE

Erkan Senses

National Institute of Standards and Technology

18 PUBLICATIONS **61** CITATIONS

SEE PROFILE

Pinar Akcora

Stevens Institute of Technology

50 PUBLICATIONS **612** CITATIONS

SEE PROFILE

Sanat K. Kumar

Columbia University

288 PUBLICATIONS **7,352** CITATIONS

SEE PROFILE

Macromolecules

Article

pubs.acs.org/Macromolecules

Role of Filler Shape and Connectivity on the Viscoelastic Behavior in Polymer Nanocomposites

Dan Zhao,[†] Shufan Ge,[†] Erkan Senses,[‡] Pinar Akcora,[‡] Jacques Jestin,[†,§] and Sanat K. Kumar*[,†]

[†]Department of Chemical Engineering, Columbia University, 500 West 120th Street, New York, New York 10027, United States

[‡]Department of Chemical Engineering and Materials Science, Stevens Institute of Technology, Castle Point on Hudson, Hoboken, New Jersey 07030, United States

[§]Laboratoire Léon Brillouin, CEA Saclay, 91191 Gif-sur-Yvette, Cedex, France

Supporting Information

ABSTRACT: We compare the rheological behavior of three classes of polymer nanocomposites (PNCs) to understand the role of particle shape and interactions on mechanical reinforcement. The first two correspond to favorably interacting composites formed by mixing poly(2-vinylpyridine) with either fumed silica nanoparticles (NPs) or colloidal spherical silica NPs. We show that fumed silica NPs readily form a percolated network at low NP volume fractions. We deduce that the NPs act as network junctions with the effectively irreversibly bound polymer chains serving as the connecting bridges. By comparing with colloidal spherical silica, which has a significantly higher percolation threshold, we conclude that the fractal shape of the fumed silica is responsible for its unusually low percolation threshold. The third system corresponds to polystyrene grafted colloidal silica nanoparticles (PGNPs) in a polystyrene matrix. These PNCs have an even lower percolation threshold probably because the grafted chains increase the effective volume fraction of the NPs. When we take these different thickness of the polymer layers in the two cases into account (i.e., grafted layer vs adsorbed layer thickness), the percolation threshold for the fumed and the grafted system occurs at similar effective loadings, but the NP network with fumed silica has a higher low-frequency plateau modulus than that formed with the PGNPs. These findings can be reconciled by the fact that the fumed silica NPs are composed of fused entities, thus ensuring that they have a higher modulus than the PGNPs where the modulus is largely attributed to interactions between the grafts. Our results systematically stress the important role of the nanofiller shape and connectivity on the mechanical reinforcement of PNCs.

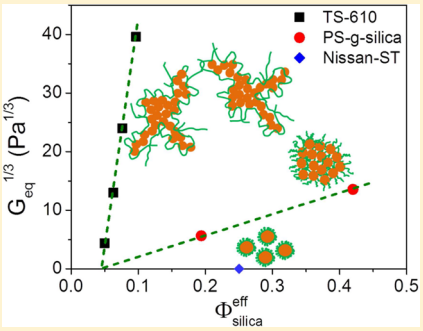

INTRODUCTION

The incorporation of nanoparticles (NPs) into a polymer matrix frequently enhances the mechanical properties, particularly the viscoelastic behavior, of the base resin.[1−5] To optimize mechanical performance in the molten state, there needs to be a pathway for stress to be propagated across the system. Several mechanisms have been proposed to understand the formation of this "percolated" state, including direct NP−NP aggregates,[6,7] percolation through bound polymer chains (including direct bridging of adsorbed chains or by the interactions between chains adsorbed on different NPs),[1,8,9] or through graft−graft adhesions in the case of polymer grafted nanoparticles (PGNPs, including direct graft−graft interactions or indirect interactions involving matrix chains).[7,10,11] Resolving between these hypotheses, which presumably depends on the type of nanofiller used, is a topic of considerable interest. On the other hand, it is now commonly accepted that the size, shape, and spatial organization of NPs in a matrix play important roles in determining the mechanical properties of the PNCs.[6,10−13] Therefore, it is critical to compare the mechanical performance of PNCs loaded with different types of NPs, including fumed, colloidal, or polymer grafted NPs. By doing this, mechanical reinforcement resulting from different mechanisms can be evaluated.

In this paper we have systematically compared the rheological behavior of nanocomposites formed with three different types of common nanofillers, i.e., fumed, colloidal spherical, and polymer grafted silica NPs, in the same or rheologically similar polymer matrices. On the basis of these results, we attempt to give some insights into the following interrelated questions: (i) What is the role of the bound/grafted polymer chains in determining the threshold beyond which solid-like rheological behavior is found? Which system results in a higher modulus and why? (ii) What role does NP shape (spherical or fractal) play in determining the onset of solid-like response in these composites? (iii) How does nanofiller shape or connectivity affect the mechanical reinforcement of the resulting PNCs?

Received: May 5, 2015
Revised: June 24, 2015
Published: July 31, 2015

DOI: 10.1021/acs.macromol.5b00962
Macromolecules 2015, 48, 5433−5438

EXPERIMENTAL SECTION

Materials. All materials were used as received. The solvents *N*,*N*-dimethylformamide (DMF, anhydrous, 99.8%) and methyl ethyl ketone (MEK or 2-butanone, HPLC grade >99.7%) were purchased from Sigma-Aldrich. Poly(2-vinylpyridine) (P2VP, M_w = 105 kg/mol, M_w/M_n = 1.08) was obtained from Polymer Source. The colloidal (MEK-ST, 10−15 nm in diameter, denoted as "Nissan-ST") and fumed (TS-610, surface treated with dimethyldichlorosilane, with an average aggregate length of 200−300 nm and a specific surface area of 125 m^2/g) silica NPs were donated by Nissan Chemical Industries and Cabot, respectively. Note that both NPs are partially surface treated but still have silanol groups available at the surface. Antioxidant Irganox 1010, donated by Ciba Specialty Chemicals (now BASF Switzerland), was used to minimize thermal degradation during annealing at high temperatures.

Nanocomposites Preparation and Processing. Nanocomposite films were prepared by cocasting composite dispersions consisting of TS-610 or Nissan-ST NPs and P2VP dissolved in DMF or MEK, following the protocol reported in our previous work.[14] In the case of TS-610, the as-received powered fumed silica NPs were first dissolved in DMF and then subjected to bath sonication for 2 min prior to mixing with the polymer solution. In order to provide precisely identical sample history and completely remove all the residual solvents in the films, a well-defined annealing procedure was adopted: 2 days at 80 °C, then 5 days at 150 °C, and finally 2 h at 180 °C, all under vacuum.

Dynamic and Static Light Scattering (DLS and SLS). The light scattering experiments were conducted on a BI-200SM (Brookhaven Instruments) instrument equipped with diode-pumped solid state (DPSS) laser operating at λ = 532 nm and a BI-9000 AT digital correlator. In a typical DLS/SLS experiment, a silica dispersion containing 0.13 wt % NP (or ∼0.048 vol %) was prepared, bath sonicated, and then filtered with a 0.45 μm PTFE filter prior to each measurement. From the DLS experiments, the hydrodynamic radius (R_H) of the test particle suspension can be estimated. First, the effective diffusion coefficient (D_{eff}) was measured at varying scattering vectors (q). The extrapolation of D_{eff} to q = 0 yields the mutual diffusion coefficient (D_0), from which R_H can be obtained following the Stokes−Einstein relation (eq 1 in the Supporting Information). SLS experiments help to determine the radius of gyration (R_G) as well as the fractal dimension (D) of the NPs. We first recorded the scattering intensity $I(q)$ as a function of the scattering angle (ranging from 15° to 150°) and then converted it to the absolute scattering intensity or Rayleigh ratio $R(q)$ using toluene as reference (eq 2 in the Supporting Information). A Guinier fit in the low q regime and a power-law fit in the intermediate q regime respectively lead to estimates of R_G and D. The details of DLS and SLS are presented in the Supporting Information.

Thermogravimetric Analysis (TGA). TGA experiments were used to quantitatively determine the amount of "bound" polymer chains on the particle surface. First, the annealed PNC film was redissolved in the casting solvent. The resulting solution was then centrifuged at 9700 rpm for 30 min. The particles with the bound P2VP formed a pellet at the bottom of the centrifuge tube, and the free P2VP remained in the supernatant. This washing and centrifuging process was repeated three times to ensure complete removal of unbound P2VP chains. The pellet obtained was dried in a 150 °C vacuum oven for 2 h and then burned in a TGA in a heating program defined as follows: isothermal at 30 °C for 2 min, a temperature ramp from 30 °C to 150 °C at a heating rate of 20 °C/min, isothermal at 150 °C for 10 min (to completely remove all the residual solvent and water), and another temperature ramp from 150 °C to 1000 °C at a heating rate of 10 °C/min. As the silica does not burn off, the weight loss in the burning process should reflect the amounts of the bound P2VP. (A "pure" silica system was used to determine that essentially nothing was burned off in this case.) The bound layer thickness was estimated based on the specific surface area of the particles as well as the mass loss determined by TGA and assuming a uniform thickness of the bound layer with a density equal to that of the neat P2VP melt.

Transmission Electron Microscopy (TEM). To characterize the particle dispersion in real space, a strip of bulk PNC film was embedded in an epoxy resin, cured at 80 °C for 8 h, and then cut into thin slices of thickness ∼60 nm at room temperature using ultramicrotomy. The resulting slices were then floated on a Formvar-coated copper TEM grid from deionized water and visualized in a Jeol JEM-100 CX electron microscope.

Rheology. Rheology experiments were conducted on a strain-controlled ARES-G2 rheometer (TA Instruments) equipped with 8 mm parallel plates. The samples were first annealed according to the protocol mentioned earlier and then compression molded into 8 mm disks using a custom molding apparatus. All rheology measurements were performed at 180 °C (∼80 °C above the T_g of neat P2VP) under nitrogen. To ensure the data were collected in a linear regime, we first ran a strain-sweep experiment at the maximum frequency covered in our study, i.e., 100 rad/s, from where the range of linear strains can be determined (Figure S5 in Supporting Information).

RESULTS AND DISCUSSION

We study three different classes of PNCs. The first two are formed from two kinds of silica NPs and P2VP as the matrices. In the first case we used TS-610 as the nanofiller. TS-610 was received in a powder form, which contains fused clusters of primary spherical particles of ∼10−20 nm in diameter.[8,15] These clusters or aggregates are the primary structure of TS-610- these cannot be broken up during the solvent casting process as the primary particles inside one cluster are fused together. Because of the manufacturing process, these particle clusters exhibit a large specific surface area and a fractal structure (see TEM images, Figure 1). Second, we used

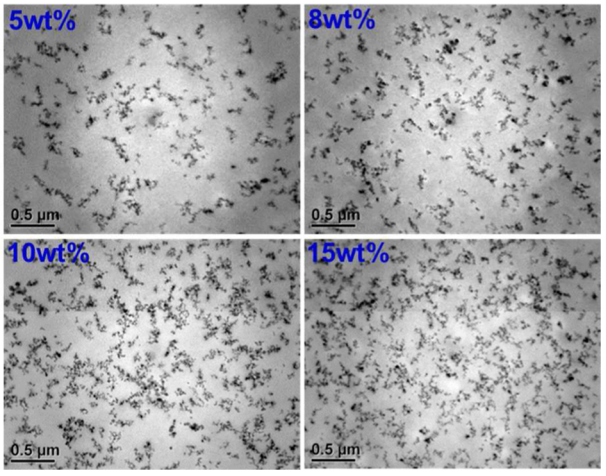

Figure 1. TEM micrographs for PNCs consisting of 105 kg/mol P2VP and TS-610 with varying loadings.

colloidal spherical silica NPs, i.e., Nissan-ST, with a diameter of 14 ± 4 nm. The Nissan-ST NPs are dispersed in MEK where they are stabilized against agglomeration by negative surface charges. According to our previous studies,[14,16,17] the favorable interaction between silica and P2VP facilitates the formation of a bound polymer layer in the melt. Note that the entanglement molecular weight (M_e) of P2VP is ∼27 kg/mol,[18,19] and the unperturbed radius of gyration (R_G) for a 105 kg/mol P2VP is ∼7.7 nm ($R_G = 6^{-1/2} bN^{1/2}$, with b = 0.6 nm and N = 1000). We defer the discussion of the third system, composed of Nissan-ST NPs grafted with polystyrene (PS) chains in a PS matrix, to later in the paper—in contrast to the P2VP, the PS does not have a favorable interaction with the silica and hence does not form a bound layer.

DOI: 10.1021/acs.macromol.5b00962
Macromolecules 2015, 48, 5433−5438

We first combine dynamic and static light scattering to examine the structural properties of TS-610 and also its stability in the casting solvent DMF. Because of the fractal, anisotropic nature of TS-610, the effective diffusion coefficient depends on the scattering vector q. An extrapolation to zero q gives a hydrodynamic radius (R_H) of ∼164 nm (Figure S1a in Supporting Information).[20] For the same reason, the characteristic time τ varies as $q^{-2.25\pm0.015}$ instead of q^{-2} expected for a purely translational, diffusive process (Figure S1b in Supporting Information). In other words, the progressive contribution of the rotational diffusion to the relaxation of the intensity correlation function at higher q leads to a faster decay in τ with q. Additionally, using SLS (Figure S2 in Supporting Information), we found (i) the fractal dimension of TS-610 is ∼1.8, a typical value for structures formed by a diffusion-limited cluster aggregation process,[21] and (ii) the R_G of TS-610 is ∼170 nm obtained from a Guinier fit in the low q regime.[20] Note that $R_G/R_H \sim 1.04$ is consistent with the elongated character of this particle. Finally, we stress that the suspensions of TS-610 in DMF are temporally stable over our experimental time scale (the stability is confirmed over 3 days; see Figure S3 in Supporting Information).

We then characterize the interaction between TS-610 and P2VP in nanocomposites, as this is critical to both the NP dispersion and the reinforcement mechanism. Presumably, as TS-610 is only partially treated, i.e., many surface silanol groups are still present, it can interact strongly with the P2VP chains (hydrogen bonding or other polar interactions)[22−24] and thereby create a bound polymer layer at the particle surface. To justify this, we measured the quantity of the bound polymer on the TS-610 surface. Specifically, we first dissolved the annealed PNCs with a silica loading of 15 wt % in DMF and then repeatedly centrifuged and solvent-washed them. TGA was then used to characterize the mass of bound P2VP (Figure S4 in Supporting Information), from which we obtained a bound layer thickness of ∼0.7 nm, assuming that it has the same density as the melt. We therefore conclude that there exists favorable interactions between TS-610 and P2VP, which facilitates the formation of a bound layer of P2VP on the NP surface.

We now examine the structure and the resulting viscoelastic properties of PNCs filled with these P2VP-adsorbed fumed silica NPs. Figure 1 presents TEM micrographs of PNCs formed with 105 kg/mol P2VP matrices and TS-610 with varying NP loadings. Clearly, the fumed NPs, which are themselves fractal clusters, are homogeneously distributed in the polymeric hosts, without large agglomerates. At low NP loadings, such as 5 wt %, TS-610 clusters are apparently individually dispersed, with no remarkable cluster−cluster overlap. With increasing silica loading, these individual fumed NP clusters start to contact each other. Visually, "percolation" appears at ∼10 wt %.

Next, we performed linear rheology experiments on these PNCs (Figure S5 in Supporting Information). The storage modulus (G') and loss modulus (G'') as a function of the probed angular frequency (ω, ranging from 10^{-3} to 10^{2} rad/s) are presented in Figure 2. Note that all the experiments were conducted at a temperature of 180 °C under nitrogen. For reference, we start with the viscoelastic properties of neat P2VP. At high frequency, the plateau in G' is associated with the entanglement behavior of high molecular weight chains. The plateau modulus (G_N^0) at ω = 100 rad/s is ∼112 000 Pa, close to the ∼132 000 Pa reported by Takahashi et al.[19] Based

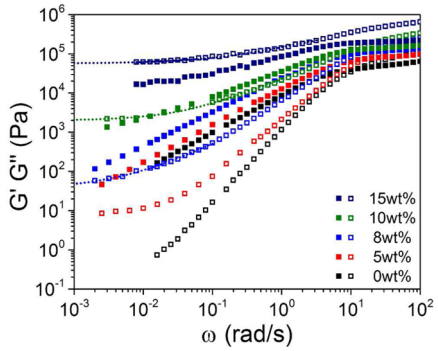

Figure 2. Linear storage (G', open symbols) and loss (G'', closed symbols) modulus recorded as a function of angular frequency (ω) at 180 °C for P2VP melts filled with TS-610 of different loadings. The dotted lines are fittings to a logistic function to obtain the extrapolated low frequency storage plateau modulus (G_{eq}). The upper limits in frequency used for logistic fittings are determined by the maximum of the loss angle (Figure S6 in Supporting Information). Note that for clarity the data from the 12 wt % PNC is not shown here.

on this, the M_e for P2VP is estimated to be ∼36 kg/mol ($M_e = \rho RT/G_N^0$), also comparable to the well-known value of ∼27 kg/mol. The observed difference in M_e should be largely due to the uncertainty in the determination of the plateau modulus. Additionally, the crossover frequency of G' and G'' implies a reptation relaxation time of ∼0.48 s for neat P2VP. At lower frequencies, G' decreases as $\omega^{1.92\pm0.05}$ and G'' ∼ $\omega^{0.96\pm0.002}$, consistent with a polymer melt. Note that the slight deviation of the exponents from the classical value of 2 and 1 presumably results from matrix polydispersity.

Figure 2 clearly shows that both G' and G'' are progressively increased with silica loading over all frequencies covered. Specifically, in the regime of matrix entanglement, the plateau modulus at ω = 100 rad/s (Figure 3a) follows the Guth equation[25]

$$G' = G'_{P2VP}[1 + 0.67\alpha\Phi_{silica} + 1.62(\alpha\Phi_{silica})^2] \quad (1)$$

where α is a shape factor (length/width) and is determined to be ∼19 by fitting to the experimental data. Note that the R_G of the TS-610 is estimated to be ∼170 nm, while the diameter of the individual NP in the fumed cluster is ∼10−20 nm. Consequently, we would expect such large shape factors only if the clusters were truly rods and not objects with fractal dimension of ∼1.8. This unexpectedly large value of α might reflect contributions from the loosely packed structure of these fractal clusters, i.e., the compactness of the objects, as has been suggested in previous works.[26] In fact, a similar value for α, i.e., 22, was reported previously for fumed silica-based nanocomposites.[27]

Going further, in the low frequency regime, mechanical reinforcement becomes much more pronounced, with the terminal flow times becoming significantly retarded with increasing silica loading. As expected, we see a second, low-frequency plateau in G' (denoted as G_{eq} below) at a silica weight fraction of 15% (∼8.11 vol %), 12% (∼6.38 vol %), and 10% (∼5.26 vol %), with possibly a plateau at 8 wt % (∼4.17 vol %). It is difficult to go to higher loadings since the material can no longer be reliably loaded into the rheometer. This frequency-independent, nonterminal behavior of G' at low frequencies is indicative of a solid-like response. It is likely that the percolated network comes from silica NPs connected by the bound P2VP chains, which serve as the network strands.

DOI: 10.1021/acs.macromol.5b00962
Macromolecules 2015, 48, 5433−5438

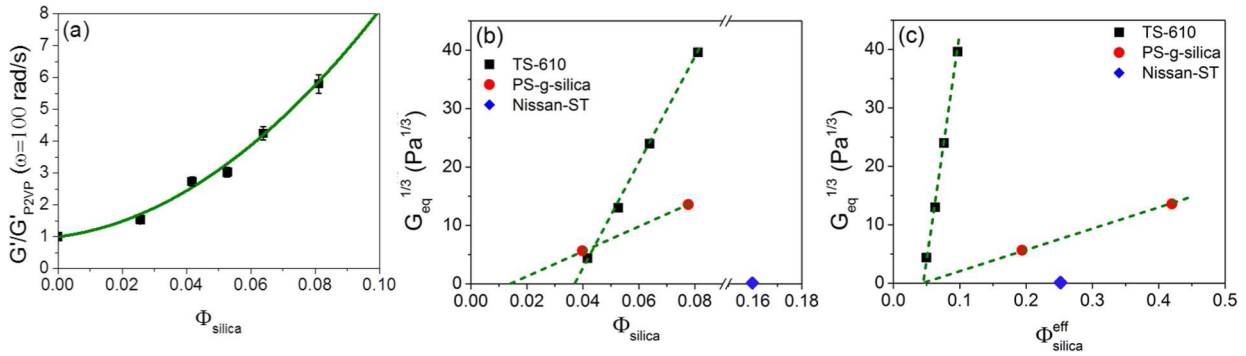

Figure 3. (a) Normalized matrix entanglement plateau storage modulus (G') at a (high) frequency of 100 rad/s for TS-610 filled PNCs as a function of silica volume fraction Φ_{silica}. The solid green line is a fit to the Guth equation. (b) Cube root of G_{eq} for both TS-610 (black squares) and PS-*g*-silica (red circles, from ref 11) filled PNCs at different volume fractions of silica NPs. (c) $G_{eq}^{1/3}$ is plotted against the effective silica NP volume fraction (Φ_{silica}^{eff}), which accounts for the volume of the bound and grafted polymer chains for the fumed/colloidal and grafted systems, respectively. The dashed green lines are piecewise linear fits of these (limited) data. Also, the percolation volume fraction (~0.16) and effective volume fraction (~0.25) for the Nissan-ST system are shown in (b) and (c), respectively. Note that the percolation volume fraction of the colloidal nanocomposites is determined by a two-phase analytical model in which the NP contribution is modeled based on critical percolation while the polymer phase contributes hydrodynamically.[28] The error bar in (b) and (c) is smaller than the symbol size.

However, this apparently contradicts TEM observations (Figure 1), especially for the 8 wt % composite, where the NP aggregates are not visually percolated. We believe this can be reconciled by the much smaller thickness of the microtomed slices (~60 nm) than the size of one NP aggregate (200−300 nm). That is the apparent concentration of NP aggregates observed in the TEM is largely reduced when some parts of the clusters are cut during microtoming. Alternatively, there is evidence that the mechanical percolation could occur at much lower NP loadings than structural percolation when the particle and the polymer strongly interact.[2,13,29] In such cases, it has been suggested the NPs could be strongly bridged with the adsorbing polymer chains, thus forming a temporary polymer−particle network at remarkably low NP content. Going further, for the 10 wt % PNC, the G' and G'' crossover again at a frequency of 0.023 rad/s and G' starts to dominate over G'' at lower frequencies. For PNCs with higher loadings, such as 15 wt %, the G' is always higher than G'', implying the dominance of solid-like response over all probed time scales. While we therefore trust the three higher loadings as being solid-like in their response, the 8 wt % sample is much less clear and must therefore be viewed with some caution. We have ruled out the data point at 5 wt % in estimation of the percolation threshold as the particles in this sample are far from structural percolation (Figure 1), thus making it essentially still behave like liquid (G' is 1 order of magnitude smaller than G'') at the lowest frequency probed.

The onset behavior of this solid-like response, or the "percolation threshold", in fumed silica nanocomposites can be quantitatively evaluated by resorting to rubber elasticity theory.[30] We use the mean-field rubber elasticity theory which suggests that $G_{eq} \sim (\phi - \phi_c)^3$. From here, we plot $G_{eq}^{1/3}$ versus the volume fraction of the silica NPs (Figure 3b). We extrapolate $G_{eq}^{1/3}$ down to a modulus of zero to obtain the onset of gelation, which is found to be 3.7 vol % (~7.1 wt %).

To understand the remarkably low percolation threshold observed for fumed silica nanocomposites, we performed the following, simple estimation. We assume that the TS-610 NPs are uniformly distributed in the P2VP matrix, and thus each aggregate occupies a volume defined by its size, R_G. The critical volume fraction above which the neighboring aggregates start to overlap ("semidilute" crossover) is given by

$$\Phi_c = (R_G/a)^{D-3} \quad (2)$$

where a is the radius of the primary particle, i.e., ~5−10 nm, and D = 1.8 is the fractal dimension. On this basis, we estimate the maximum packing volume fraction to be ~1.5−3.3 vol %, close to the gel point predicted by the rubber elasticity theory. The similar values of the maximum packing density and percolation threshold for this fumed system should result from the individual, homogeneous dispersion of silica aggregates in the P2VP matrices. In fact, Cassagnau et al.[31] have reported a percolation threshold of 3.3 vol % for fumed silica nanocomposites. Consequently, the unusually low percolation threshold for fumed silica nanocomposites should be largely attributed to the fractal, open structure of the TS-610 aggregates.

This argument can be substantiated by comparing the rheological behavior of PNCs filled with TS-610 fumed silica NPs and colloidal spherical silica NPs. Two facts are apparent in Figure 4. First, over all frequencies considered, both G' and G'' for the TS-610 filled PNC are higher than that for Nissan-ST. Second, at lower frequencies, we observe a secondary plateau in the fumed nanocomposite while in the colloidal case the test material starts to behave like liquid ($G' < G''$). Notably, the terminal slopes for the colloidal sample have not been

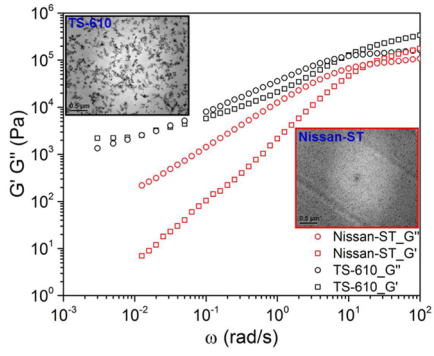

Figure 4. Storage (G') and loss (G'') modulus as a function of angular frequency collected at 180 °C for 105 kg/mol P2VP melts filled with 10 wt % TS-610 fumed silica NPs (black) or Nissan-ST NPs (red). Also included are the TEM micrographs for these two PNCs.

DOI: 10.1021/acs.macromol.5b00962
Macromolecules 2015, 48, 5433−5438

reached up to the lowest frequency probed, suggesting that the particle structures, presumably particles bridged by polymer chains, have not yet fully relaxed.[13] This low frequency reinforcement can be well described by our recent work in which the NP contribution is modeled using critical percolation.[28] In fact, the percolation threshold for the colloidal system is predicted to be ∼16 vol %,[28] significantly larger than that in the fumed case (Figure 3b). The predicted percolation volume fraction for our colloidal system is close to the value of ∼15 vol % for noninteracting spheres.[32] Note that the primary particle diameter of TS-610 is ∼10−20 nm, roughly equal to that of the colloidal silica considered here, i.e., ∼14 nm. In other words, the colloidal PNCs can be considered as a limiting case where the fumed NPs are "unfumed" and then well-dispersed in the same matrix. Clearly, the large fractal, loosely packed aggregates give a much lower percolation threshold but a significantly higher reinforcement than the small individual particles, as similarly observed by previous researchers.[33,34] These results thus emphasize the importance of the shape, connectivity, and structural openness of the nanofiller in the context of its efficiency for mechanical reinforcement.

We finally recall that in our previous work on PNCs filled with PS grafted silica (PS-*g*-silica, with a grafting density of 0.05 chains/nm^2) NPs[11], we also observed a percolated polymer−particle network "connected" in this case by the grafting chains. For the grafted system, according to the rubber elasticity theory (Figure 3b), the low frequency sol−gel transition is determined to be ∼1.5 vol % (or 3.2 wt %), more than 2 times smaller than that found for fumed PNCs. We conjecture that the lower percolation threshold for the grafted system partly results from the presence of the grafted chains,[35] which effectively increases the volume fraction of the NPs. This is justified by Figure 3c, where the percolation threshold is calculated to roughly be the same for these two systems when the effective silica volume fraction is used, i.e., the bound and grafted polymer chains, respectively, are regarded as part of the particle phase for the fumed and grafted systems. The bound layer thickness used for determination of $\Phi^{\mathrm{eff}}_{\mathrm{silica}}$ is 0.7 and 1.1 nm,[28] respectively, for the fumed and colloidal PNCs. For the grafted system, the brush thickness is estimated to be ∼4.9 nm (with a grafted chain length of 114 kg/mol and grafting density of 0.05 chains/nm^2) and ∼5.4 nm (with a grafted chain length of 150 kg/mol and grafting density of 0.05 chains/nm^2) respectively for the low and high loading PNCs shown in Figure 3b, assuming its mass density equal to a neat PS melt.

Another fact to be noted from Figure 3b is that at high silica content the polymeric melts are more reinforced by the TS-610 fumed silica NPs than the grafted ones. According to the simple argument following from the rule of mixtures, the strength of the composite material depends on the strength of its components. Effectively, the fumed nanocomposites are formed by fumed silica aggregates and the matrix polymer chains while the grafted ones consist of connected/sheets structures (comprising of PGNPs) and the bulk polymer phase. Apparently, our finding can be simply attributed to the much stronger silica−silica adhesion (chemical bonding) in a fumed aggregate than that between the graft−graft chains (chain−chain entanglement or interpenetration), as similarly observed by Chevigny et al.[36] Note that our finding cannot be attributed to the deformability of the grafted chains for two reasons. First, the rheological experiments were run in a linear regime. Thus, the deformation applied is sufficiently small that the polymer chains remain close to their equilibrium state. Moreover, in the low frequency regime where the G_{eq} is extrapolated, the polymer chains should have already fully relaxed. We thus conclude that compared to grafted NP filled PNCs, those containing fumed silica NPs have a higher mechanical reinforcement.

Let we propose criteria for designing appropriate PNCs with desired properties. When one desires to maximize the mechanical reinforcement of the polymer melt, fumed silica NPs should be the optimal filler, since they percolate at remarkably low volume fraction and give rise to highest modulus. The PGNPs, although less reinforced compared to the fumed analogues, have the advantage that particle structures can be facilely controlled by varying the grafting density and chain length, thus providing a way to manipulate the mechanical or other physical properties of the resulting PNCs.[11,37] Going further, for other applications, one might need strengthened materials with good insulation properties but minimized optical scattering. In such cases, the colloidal spherical silica could be the desired filler. As a concluding remark, our results consistently suggest that the interfacial interactions, including filler−filler and filler−polymer, are critical to optimizing the macroscopic properties of PNCs. Current efforts are made in our laboratories to examine the role of interfacial structure and interaction on the physical characteristics of PNCs with well-controlled particle morphologies.

CONCLUSION

In summary, we investigated the dispersion structure of TS-610 in a P2VP matrix and related it to the resulting linear viscoelastic properties of the nanocomposite. From rheology, we showed that the TS-610 readily forms a percolated network at a remarkably low volume fraction, with NPs acting as network junctions while the bound polymer chains serving as the connecting bridges. Following that we compared the rheological behavior of PNCs filled with different types of NPs, i.e., fumed (I), colloidal (II), and polymer-grafted (III) silica NPs. Comparing (I) and (II), we have shown the important role of the shape, connectivity, and structural openness of the nanofiller on its reinforcement capacity, evidenced by solid-like behavior at low frequencies and the larger storage modulus over all probed time scales in fumed silica nanocomposites. Finally, comparing (I) and (III), we have found (i) an apparently lower percolation threshold for (III) presumably resulting from the presence of the grafted polymer chains and (ii) a larger low frequency plateau modulus at high silica content for (I), which should be a consequence of the stronger adhesion between silica−silica in a fumed NP than that between graft−graft chains.

ASSOCIATED CONTENT

Supporting Information

Dynamic and static light scattering, detailed structural characterization for TS-610, stability of TS-610 in DMF, TGA curves for TS-610 with or without adsorbed P2VP chains, strain sweep results, loss angle vs frequency. The Supporting Information is available free of charge on the ACS Publications website at DOI: 10.1021/acs.macromol.5b00962.

AUTHOR INFORMATION

Corresponding Author

*E-mail: sk2794@columbia.edu (S.K.K.).

DOI: 10.1021/acs.macromol.5b00962
Macromolecules 2015, 48, 5433−5438

Notes

The authors declare no competing financial interest.

■ ACKNOWLEDGMENTS

The authors are grateful to the National Science Foundation (DMR-1408323) for financial support of this work.

■ REFERENCES

(1) Yurekli, K.; Krishnamoorti, R.; Tse, M. F.; McElrath, K. O.; Tsou, A. H.; Wang, H. C. *J. Polym. Sci., Part B: Polym. Phys.* **2001**, *39*, 256−275.
(2) Zhang, Q.; Archer, L. A. *Langmuir* **2002**, *18*, 10435−10442.
(3) Cassagnau, P. *Polymer* **2008**, *49*, 2183−2196.
(4) Kumar, S. K.; Jouault, N.; Benicewicz, B.; Neely, T. *Macromolecules* **2013**, *46*, 3199−3214.
(5) Sternstein, S.; Zhu, A. J. *Macromolecules* **2002**, *35*, 7262−7273.
(6) Payne, A. R. *J. Appl. Polym. Sci.* **1965**, *9*, 2273−2284.
(7) Bartholome, C.; Beyou, E.; Bourgeat-Lami, E.; Cassagnau, P.; Chaumont, P.; David, L.; Zydowicz, N. *Polymer* **2005**, *46*, 9965−9973.
(8) Aranguren, M. I.; Mora, E.; DeGroot, J. V., Jr.; Macosko, C. W. *J. Rheol.* **1992**, *36*, 1165−1182.
(9) Maier, P. G.; Göritz, D. *Kautsch. Gummi Kunstst.* **1996**, *49*, 18−21.
(10) Akcora, P.; Kumar, S. K.; Moll, J.; Lewis, S.; Schadler, L. S.; Li, Y.; Benicewicz, B. C.; Sandy, A.; Narayanan, S.; Ilavsky, J.; Thiyagarajan, P.; Colby, R. H.; Douglas, J. F. *Macromolecules* **2010**, *43*, 1003−1010.
(11) Moll, J. F.; Akcora, P.; Rungta, A.; Gong, S.; Colby, R. H.; Benicewicz, B. C.; Kumar, S. K. *Macromolecules* **2011**, *44*, 7473−7477.
(12) Akcora, P.; Kumar, S. K.; García Sakai, V.; Li, Y.; Benicewicz, B. C.; Schadler, L. S. *Macromolecules* **2010**, *43*, 8275−8281.
(13) Jouault, N.; Vallat, P.; Dalmas, F.; Said, S.; Jestin, J.; Boué, F. *Macromolecules* **2009**, *42*, 2031−2040.
(14) Jouault, N.; Zhao, D.; Kumar, S. K. *Macromolecules* **2014**, *47*, 5246−5255.
(15) Barthel, H. *Colloids Surf., A* **1995**, *101*, 217−226.
(16) Harton, S. E.; Kumar, S. K.; Yang, H.; Koga, T.; Hicks, K.; Lee, H.; Mijovic, J.; Liu, M.; Vallery, R. S.; Gidley, D. W. *Macromolecules* **2010**, *43*, 3415−3421.
(17) Jouault, N.; Moll, J. F.; Meng, D.; Windsor, K.; Ramcharan, S.; Kearney, C.; Kumar, S. K. *ACS Macro Lett.* **2013**, *2*, 371−374.
(18) Beck Tan, N. C.; Peiffer, D. G.; Briber, R. M. *Macromolecules* **1996**, *29*, 4969−4975.
(19) Takahashi, Y.; Ochiai, N.; Matsushita, Y.; Noda, I. *Polym. J.* **1996**, *28*, 1065−1070.
(20) Kätzel, U.; Vorbau, M.; Stintz, M.; Gottschalk-Gaudig, T.; Barthel, H. *Part. Part. Syst. Charact.* **2008**, *25*, 19−30.
(21) Lin, M. Y.; Lindsay, H. M.; Weitz, D. A.; Ball, R. C.; Klein, R.; Meakin, P. *Proc. R. Soc. London, Ser. A* **1989**, *423*, 71−87.
(22) Utracki, L. A.; Jamieson, A. M. *Polymer Physics: From Suspensions to Nanocomposites and Beyond*; John Wiley & Sons: New York, 2011.
(23) Holt, A. P.; Sangoro, J. R.; Wang, Y.; Agapov, A. L.; Sokolov, A. P. *Macromolecules* **2013**, *46*, 4168−4173.
(24) Holt, A. P.; Griffin, P. J.; Bocharova, V.; Agapov, A. L.; Imel, A. E.; Dadmun, M. D.; Sangoro, J. R.; Sokolov, A. P. *Macromolecules* **2014**, *47*, 1837−1843.
(25) Guth, E. *J. Appl. Phys.* **1945**, *16*, 20−25.
(26) Wu, Y. P.; Jia, Q. X.; Yu, D. S.; Zhang, L. Q. *Polym. Test.* **2004**, *23*, 903−909.
(27) Song, Y.; Zheng, Q. *Polymer* **2010**, *51*, 3262−3268.
(28) Chen, Q.; Gong, S.; Moll, J.; Zhao, D.; Kumar, S. K.; Colby, R. H. *ACS Macro Lett.* **2015**, *4*, 398−402.
(29) Bouty, A.; Petitjean, L.; Degrandcourt, C.; Gummel, J.; Kwaśniewski, P.; Meneau, F.; Boué, F. o.; Couty, M.; Jestin, J. *Macromolecules* **2014**, *47*, 5365−5378.
(30) Rubinstein, M.; Colby, R. H. *Polymer Physics*; Oxford University Press: Oxford, UK, 2003.
(31) Cassagnau, P. *Polymer* **2003**, *44*, 2455−2462.
(32) Scher, H.; Zallen, R. *J. Chem. Phys.* **1970**, *53*, 3759−3761.
(33) Wypych, G. *Handbook of Fillers*; ChemTec Publishing: Toronto, 1999.
(34) Niu, R.; Gong, J.; Xu, D.; Tang, T.; Sun, Z. Y. *RSC Adv.* **2014**, *4*, 62759−62768.
(35) Goel, V.; Chatterjee, T.; Bombalski, L.; Yurekli, K.; Matyjaszewski, K.; Krishnamoorti, R. *J. Polym. Sci., Part B: Polym. Phys.* **2006**, *44*, 2014−2023.
(36) Chevigny, C.; Jouault, N.; Dalmas, F.; Boué, F.; Jestin, J. *J. Polym. Sci., Part B: Polym. Phys.* **2011**, *49*, 781−791.
(37) Akcora, P.; Liu, H.; Kumar, S. K.; Moll, J.; Li, Y.; Benicewicz, B. C.; Schadler, L. S.; Acehan, D.; Panagiotopoulos, A. Z.; Pryamitsyn, V.; Ganesan, V.; Ilavsky, J.; Thiyagarajan, P.; Colby, R. H.; Douglas, J. F. *Nat. Mater.* **2009**, *8*, 354−359.

DOI: 10.1021/acs.macromol.5b00962
Macromolecules 2015, 48, 5433−5438